ISSN 1674-1056
http://cpb.iphy.ac.cn
http://iopscience.iop.org/cpb
中国物理 B
Chinese Physics
中国物理 Chinese Physics B

High performance silicon-based GeSn p-i-n photodetectors for short-wave infrared application

Yue Zhao(赵越)[1,2], Nan Wang(王楠)[1,2], Kai Yu(余凯)[1,2], Xiaoming Zhang(张晓明)[3], Xiuli Li(李秀丽)[1,2], Jun Zheng(郑军)[1,2], Chunlai Xue(薛春来)[1,2], Buwen Cheng(成步文)[1,2], Chuanbo Li(李传波)[3,4]

Citation: Chin. Phys. B . 2019, 28(12): 128501 . **doi:** 10.1088/1674-1056/ab4e84
Journal homepage: http://cpb.iphy.ac.cn; http://iopscience.iop.org/cpb

What follows is a list of articles you may be interested in

Rectifying characteristics and solar-blind photoresponse in *β*-Ga_2O_3/ZnO heterojunctions

Xiao-Fei Ma(马晓菲), Yuan-Qi Huang(黄元琪), Yu-Song Zhi(支钰崧), Xia Wang(王霞), Pei-Gang Li(李培刚), Zhen-Ping Wu(吴真平), Wei-Hua Tang(唐为华)

Chin. Phys. B . 2019, 28(8): 088503 . **doi:** 10.1088/1674-1056/28/8/088503

Ultraviolet photodetectors based on wide bandgap oxide semiconductor films

Changqi Zhou(周长祺), Qiu Ai(艾秋), Xing Chen(陈星), Xiaohong Gao(高晓红), Kewei Liu(刘可为), Dezhen Shen(申德振)

Chin. Phys. B . 2019, 28(4): 048503 . **doi:** 10.1088/1674-1056/28/4/048503

Effect of temperature on photoresponse properties of solar-blind Schottky barrier diode photodetector based on single crystal Ga_2O_3

Chao Yang(杨超), Hongwei Liang(梁红伟), Zhenzhong Zhang(张振中), Xiaochuan Xia(夏晓川), Heqiu Zhang(张贺秋), Rensheng Shen(申人升), Yingmin Luo(骆英民), Guotong Du(杜国同)

Chin. Phys. B . 2019, 28(4): 048502 . **doi:** 10.1088/1674-1056/28/4/048502

High quantum efficiency long-/long-wave dual-color type-Ⅱ InAs/GaSb infrared detector

Zhi Jiang(蒋志), Yao-Yao Sun(孙姚耀), Chun-Yan Guo(郭春妍), Yue-Xi Lv(吕粤希), Hong-Yue Hao(郝宏玥), Dong-Wei Jiang(蒋洞微), Guo-Wei Wang(王国伟), Ying-Qiang Xu(徐应强), Zhi-Chuan Niu(牛智川)

Chin. Phys. B . 2019, 28(3): 038504 . **doi:** 10.1088/1674-1056/28/3/038504

Comparison of blue-green response between transmission-mode GaAsP-and GaAs-based photocathodes grown by molecular beam epitaxy

Gang-Cheng Jiao(焦岗成), Zheng-Tang Liu(刘正堂), Hui Guo(郭晖), Yi-Jun Zhang(张益军)

Chin. Phys. B . 2016, 25(4): 048505 . **doi:** 10.1088/1674-1056/25/4/048505

High performance silicon-based GeSn p–i–n photodetectors for short-wave infrared application*

Yue Zhao(赵越)[1,2], Nan Wang(王楠)[1,2], Kai Yu(余凯)[1,2], Xiaoming Zhang(张晓明)[3], Xiuli Li(李秀丽)[1,2], Jun Zheng(郑军)[1,2], Chunlai Xue(薛春来)[1,2], Buwen Cheng(成步文)[1,2], and Chuanbo Li(李传波)[3,4,†]

[1] *State Key Laboratory on Integrated Optoelectronics, Institute of Semiconductors, Chinese Academy of Sciences, Beijing* 100083, *China*
[2] *Center of Materials Science and Opto-Electronic Engineering, University of Chinese Academy of Sciences, Beijing* 100049, *China*
[3] *School of Science, Minzu University of China, Beijing* 100081, *China*
[4] *Optoelectronics Research Center, Minzu University of China, Beijing* 100081, *China*

(Received 4 September 2019; revised manuscript received 27 September 2019; published online 15 November 2019)

An investigation of germanium-tin (GeSn) on silicon p–i–n photodetectors with a high-quality $Ge_{0.94}Sn_{0.06}$ absorbing layer is reported. The GeSn photodetector reached a responsivity as high as 0.45 A/W at the wavelength of 1550 nm and 0.12 A/W at the wavelength of 2 μm. A cycle annealing technology was applied to improve the quality of the epitaxial layer during the growth process by molecular beam epitaxy. A low dark-current density under 1 V reverse bias about 0.078 A/cm^2 was achieved at room temperature. Furthermore, the GeSn photodetector could detect a wide spectrum region and the cutoff wavelength reached to about 2.3 μm. This work has great importance in silicon-based short-wave infrared detection.

Keywords: GeSn alloy, molecular beam epitaxy, photodetector, cycle annealing

PACS: 85.60.Gz, 81.40.Ef, 61.66.Dk, 68.55.ag **DOI:** 10.1088/1674-1056/ab4e84

1. Introduction

Germanium-tin alloy (GeSn), a new group IV compound, has recently attracted significant research interest due to its good performance of tunable bandgap width[1,2] and enhanced carrier mobility compared with other group IV material or compound.[3] Research shows that the increase of Sn concentration in GeSn leads to a decrease of its bandgap width. This phenomenon extends the detection zone of the GeSn photodetector toward longer wavelengths, therefore GeSn photodetector can be utilized in short-wave infrared (SWIR) applications, including infrared imagery field, non-invasive detecting, medical diagnostics, fiber-optic telecommunications, and so on.[4–8] Furthermore, the manufacturing process of GeSn alloy is compatible with Si complementary metal oxide semiconductor (CMOS) processing technology, which shows a huge potential in silicon-based optoelectronics.[9]

However, there are significant challenges in growing high-quality GeSn materials. For example, the equilibrium solubility of Sn in Ge is lower than 1%,[10] Sn easily segregates with temperature increasing, and the lattice mismatch between Ge and α-Sn is as large as 14.7%.[11,12] In order to release the misfit dislocation between the Ge buffer and Si substrate, we adopted a two-step growth method to grow the Ge buffer all the time.[13] However, it would produce plentiful threading dislocations that can spread to the upper GeSn layer and eventually damage the quality of the upper material. In this work, we adopted multiple cycle annealing to grow high-quality GeSn alloy by molecular beam epitaxy (MBE). Multiple cycle annealing minimizes the dislocation in the Ge buffer, at the same time introduces tensile strain in the epitaxial Ge buffer.[14] This tensile strain can partially relieve the compressive strain caused by large lattice mismatch in following epitaxial GeSn layer, thus optimizing the quality of the GeSn layer.

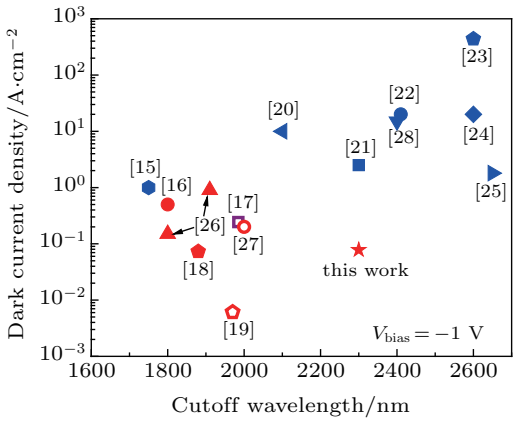


Fig. 1. Comparison of dark current density for GeSn photodetectors at a reverse bias of 1 V in different groups.[15–28] Different colors of the icons represent the different growth methods of GeSn alloy, red, purple, and blue refer to the growth methods of MBE, magnetron sputtering epitaxy, and CVD, respectively. Solid or hollow icons refer to the GeSn materials grown on Si substrate or on Ge substrate, on which devices were fabricated.

The silicon-based GeSn p–i–n photodetector was fabri-

*Project supported by the National Key Research and Development Program of China (Grant No. 2018YFB2200500), the National Natural Science Foundation of China (Grant Nos. 61675195, 61934007, and 61974170), Opened Fund of the State Key Laboratory of Integrated Optoelectronics, China (Grant No. IOSKL2018KF17), and Beijing Natural Science Foundation, China (Grant No. 4162063).

†Corresponding author. E-mail: cbli@muc.edu.cn

© 2019 Chinese Physical Society and IOP Publishing Ltd

cated with high-quality $Ge_{0.94}Sn_{0.06}$ materials. The device exhibited well-behaved diode characteristics with a low dark-current density about 0.078 A/cm^2 under 1 V reverse bias at room temperature. In addition, the spectral response of the GeSn photodetector has covered most of the SWIR wavelength, whose cutoff wavelength can reach to about 2.3 μm. High responsivities of 0.45 A/W and 0.12 A/W were achieved at the wavelengths of 1550 nm and 2 μm, respectively. As shown in Fig. 1, compared to other reported results, this work achieved better optical sensitivity by raising the optical responsivity and lowing the dark-current density. According to the detailed device analysis, the device will show the best performance under the condition of 600-nm thick, high-quality GeSn absorbing layer and multiple cycle annealing.

2. Material growth and device fabrication

2.1. Material growth and annealing

The material was grown on n-type Si (100) substrate with solid source molecular beam epitaxy. The epitaxial layer stacks consist of a 500 nm-thick Ge buffer, and a 650 nm-thick $Ge_{0.94}Sn_{0.06}$ absorbing layer grown at 180 °C. The Ge buffer was grown by a two-step growth method, composed by 100 nm-thick low temperature Ge (LT-Ge) and 400 nm-thick high temperature Ge (HT-Ge), and underwent a multiple-cycle annealing from 600 °C to 800 °C, which was designed to improve the quality of the Ge and GeSn layers. Owing to significant challenges mentioned above, growing high-quality GeSn material directly on Si substrate is difficult. Currently, we always use the high–low temperature growth method (known as two-step growth method) to grow the Ge buffer. This method can release partial misfit dislocations at the Si and Ge interface. Meanwhile, it produces plentiful threading dislocations, which will spread to the upper GeSn material and decrease the material quality. It has been proved that multiple-cycle annealing can minimize the dislocation in the Ge buffer.[14] High temperature (as close as possible, but not higher than the melting point of Ge) provides energy to the dislocations which exist in the epitaxial film, makes them migrate and ultimately quench. Furthermore, considering the different thermal expansion coefficients between Ge and Si, the epitaxial Ge buffer will induce tensile strain in cycle annealing, as shown in Table 1. This tensile strain can reduce the compressive strain in following epitaxial GeSn material, thus increasing the quality of the GeSn material.

2.2. Fabrication of device

To form p^+ $Ge_{0.94}Sn_{0.06}$ contact, the top of the GeSn layer was implanted by boron fluoride ions (BF^{2+}) with energy of 20 keV (calculated doping depth is 50 nm) and dose of 4.0 $\times 10^{15}$ cm^{-2}. In order to repair the lattice damage caused by the implantation of BF^{2+} ions and thermally activate BF^{2+} ions, the material was subsequently annealed at 450 °C for 30 s in an N_2 atmosphere. There is a temperature tradeoff between effectively lattice repairing and preventing Sn segregation. This sample was made out of circular mesas by standard photolithography and Cl-based inductively coupled plasma (ICP) etching with Cl_2, BCl_3, Ar plasma at flow rates of 10 sccm, 30 sccm, 20 sccm respectively, and 60 W RF power. These conditions realized an etch rate of 350 nm/min and produced well-defined mesas with sharp sidewalls, and smooth, residue-free surfaces.

To reduce the reflection and passivate surface of the material, a 500 nm-thick SiO_2 layer was deposited on the material by plasma-enhanced chemical vapor deposition (PECVD). The electrodes were deposited on both top-GeSn layer and Si substrate using electron beam evaporation and then fabricated by a lift-off process, including a 40 nm-thick Ni adhesion layer and a 500 nm-thick Al. Through processing mentioned above, we fabricated different mesa size devices, varying from 30 μm to 200 μm. The top-view microscopic image of the $Ge_{0.94}Sn_{0.06}$ photodetector with a 200 μm-diameter mesa is shown in Fig. 2(a).

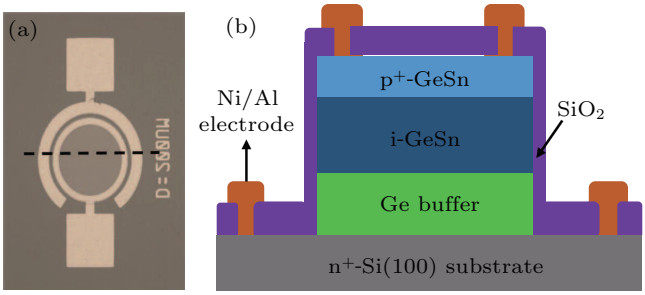


Fig. 2. (a) Top-view microscopic image of the GeSn photodetector. The mesa size is 200 μm in diameter. (b) Cross-sectional schematic of the top-illuminated GeSn photodetector structure along the black dash line shown in (a).

2.3. Characterization of material

The x-ray diffraction (XRD) ω–2θ scanning of the $Ge_{0.94}Sn_{0.06}$ sample grown on Ge buffered Si(100) substrate around (004) orientation is presented in Fig. 3(a). As we can see, the three peaks from left to right correspond to the $Ge_{0.94}Sn_{0.06}$ layer, Ge buffer, and Si substrate, respectively. At the same time, the full widths at half maximum (FWHM) of the $Ge_{0.94}Sn_{0.06}$ peak and Ge peak are 0.09° and 0.10°, respectively, which indicates that this GeSn layer has good crystalline quality. Furthermore, the substitutional Sn concentration, the lattice constant, and the strain of layer can be calculated by the same way reported in Ref. [16]. Table 1 summarizes the calculated results. It shows that the Ge buffer contains about 0.19% biaxial tensile strain, which verifies the conclusion mentioned above that the different thermal expansion coefficient between Si and Ge will introduce tensile strain in the Ge buffer.[29] This tensile strain can expand the lattice

constant of Ge, and partially relieves compressive strain in the upper GeSn layer. The relieving of compressive strain leads to the narrowing of the GeSn bandgap, and thus extends the cutoff wavelength of the detector.

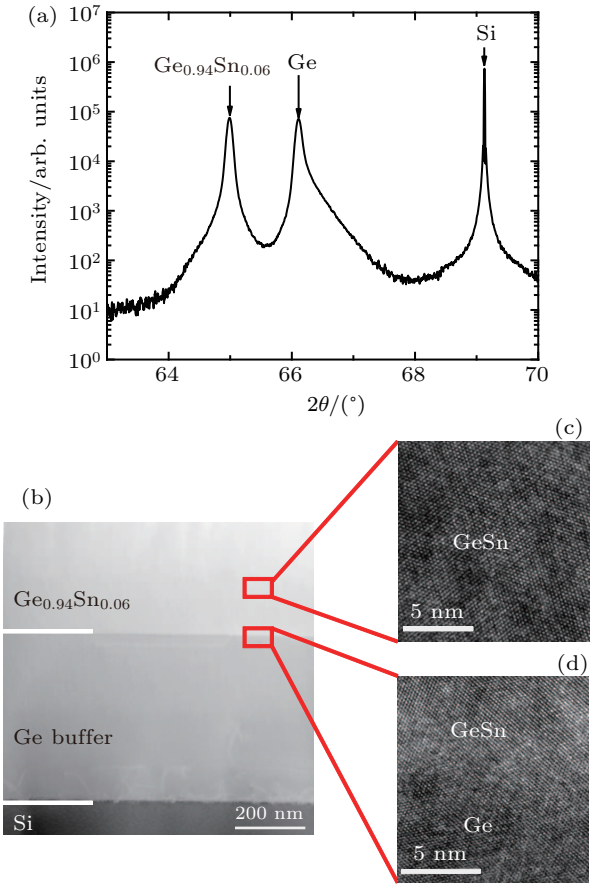


Fig. 3. HR-XRD ω–2θ scanning of the $Ge_{0.094}Sn_{0.06}$ sample grown on Ge buffered Si(100) substrate at (004) orientation. (b) TEM image of the $Ge_{0.94}Sn_{0.06}$ sample (the white lines in the image represent the interfaces of $Ge_{0.94}Sn_{0.06}$/Ge buffer and Ge buffer/Si, respectively). (c) HR-TEM image of the $Ge_{0.94}Sn_{0.06}$ layer. (d) HR-TEM image of the interface between GeSn layer and Ge buffer layer.

Table 1. Summary of lattice constant, in-plane strain, and Sn concentration.

Layer	$a_{\perp}$/Å	$a_{\parallel}$/Å	$\varepsilon_{\parallel}$/%	Sn concentration
Ge buffer	5.6489	5.6675	0.19	–
GeSn	5.7352	5.6677	–0.75	5.89%

The high resolution transmission electron microscopy (HR-TEM) image of the $Ge_{0.94}Sn_{0.06}$ on Ge buffered Si is shown in Fig. 3(b). It indicates that the $Ge_{0.94}Sn_{0.06}$ epitaxial layer is single-crystalline. In addition, a high quality interface between the Ge buffer and $Ge_{0.94}Sn_{0.06}$ layer is shown in Fig. 1(d). Compared to the TEM images that without cycling annealing (not shown here), cycle annealing truly has a positive effect on improving the material quality.

3. Results and discussion

In this work, we have adopted a series of instruments to measure the *I*–*V* characteristics, optical response, and spectral response of the $Ge_{0.94}Sn_{0.06}$ p–i–n photodetectors at room temperature respectively, such as Agilent B1500A semiconductor device analyzer, tunable laser (1500–1630 nm), 2000 nm laser, and Nicolet 6700 Fourier transform infrared (FTIR) spectrometer. In addition, a commercial InGaAs photodetector was measured to calibrate the spectral response.

3.1. Electrical characteristic of $Ge_{0.94}Sn_{0.06}$ photodetectors

The dark current–voltage (*I*–*V*) characteristics of the fabricated silicon-based $Ge_{0.94}Sn_{0.06}$ p–i–n photodetectors with different mesa sizes in diameter are shown in Fig. 4(a). It is observed that these devices exhibit a rectifying behavior of diode and the lowest dark-current of the devices with 30 μm-diameter mesa is 1.53 μA under 1 V reverse bias, which is comparably low compared to other reported values. A high I_{on}/I_{off} ratio about four orders of magnitude is measured under 1 V bias voltage, which is comparable to the reported values.[30,31]

Further analysis of the dark current density (J_{dark}) has been conducted, which can be expressed as

$$J_{dark} = J_{bulk} + \frac{4J_{surf}}{D}, \tag{1}$$

where J_{bulk} and J_{surf} are the bulk leakage current density and the peripheral surface leakage current density, respectively, and *D* is the diameter of the device mesa.

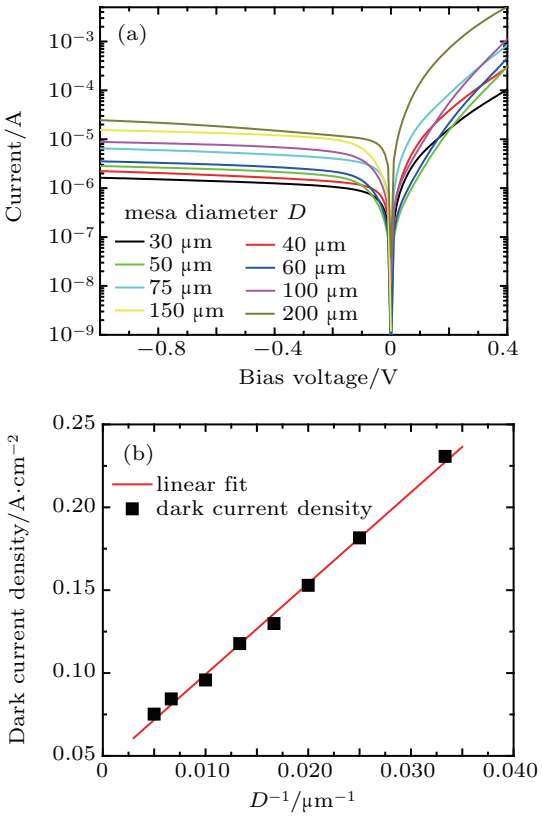


Fig. 4. (a) The I_{dark}–V_{bias} characteristics of GeSn photodetectors with various mesa sizes. (b) Dark-current density (J_{dark}) versus $1/D$ under 1 V reverse bias.

According to this formula, the J_{dark} versus $1/D$ for the GeSn photodetectors at a reverse bias of 1 V bias, where D varies from 30 μm to 200 μm, is depicted in Fig. 4(b). At the same time, J_{bulk} and J_{surf} of the photodetectors can be calculated by linearly fitting the data in the scatter plot, which are 44.29 mA/cm^2 and 0.13 mA/cm, respectively. Moreover, the 200 μm-diameter photodector obtained the lowest dark-current density 0.075 A/cm^2 under 1 V reverse bias. The J_{dark} of the GeSn photodetectors typically increases with the Sn component. Increasing Sn component will lead to the narrowing bandgap and the increasing defect density. Since J_{bulk} is proportional to the threading-dislocation density, the lower J_{bulk} can indicate the high quality of the GeSn sample processed by circle annealing.

In addition, the main source of J_{surf} is interface traps around the mesa sidewall, which can introduce energy levels in the forbidden gap and eventually increase the peripheral surface leakage current. These traps were formed in the ICP etching process of the mesa. Currently, it has been reported that the passivation technique can effectively decrease the dark current, for example, forming Si,[18] yttrium-doped GeO_2,[32] or GeO_x/$GeSnO_x$ (formed by ozone oxidation)[33] passivation layer.

3.2. Photo response characteristic of $Ge_{0.94}Sn_{0.06}$ p–i–n photodetectors

Figure 5 shows the I–V characteristics of the GeSn photodetectors (mesa diameter: 200 μm) in the dark and under the light of 1550 nm and 2000 nm laser with power of 1 mW and 0.12 mW, respectively. High responsitives of 0.45 A/W and 0.12 A/W are achieved at 1550 nm and 2000 nm under a reverse bias of 3 V, respectively, which are fairly high values for the Si-based GeSn p–i–n photodetectors as so far. The responsivity of GeSn photodetectors depends on the Sn content, the crystal quality, and the thickness of the GeSn absorbing layer. In the past few years, numerous Si-based GeSn photodetectors have been reported with relatively high responsivity ranging from 0.1 A/W to 0.376 A/W at 1550 nm.[15–28,34,35] Therefore, the 600 nm-thick high-quality GeSn absorbing layer grown by multiple cycle annealing leads to the above-mentioned high responsivity and low dark current device performance. In 2018, Huang *et al.* reported a $Ge_{0.0975}Sn_{0.025}$ resonant-cavity-enhanced photodetector (RCEPD) fabricated on silicon-on-insulator (SOI) platform. To enhance the light–matter interaction, a vertical resonant cavity is created. This leads to a clear oscillation characteristic of responsivity and peaks at 1543 nm, which is exactly in the telecommunication C-band.[34] This result shows that the responsivity of the GeSn photodetectors can be further improved by designing the resonant cavity.

The inset displays the responsivity of the devices as a function of the applied voltage at 1550 nm. We find that photon-generated carriers are efficiently collected under a reverse bias of 0.25 V. With the increase of the reverse bias voltage, the responsivity increases slowly, finally peaks at −4.22 V. As the voltage increases further, there is a modest decline in the responsivity. This phenomenon may be caused by drastically increasing leakage current under higher reverse bias voltage. What is more, it has been reported that the Franz–Keldysh effect, which refers to the absorption coefficient dependence on the voltage, could affect the responsivity.[36]

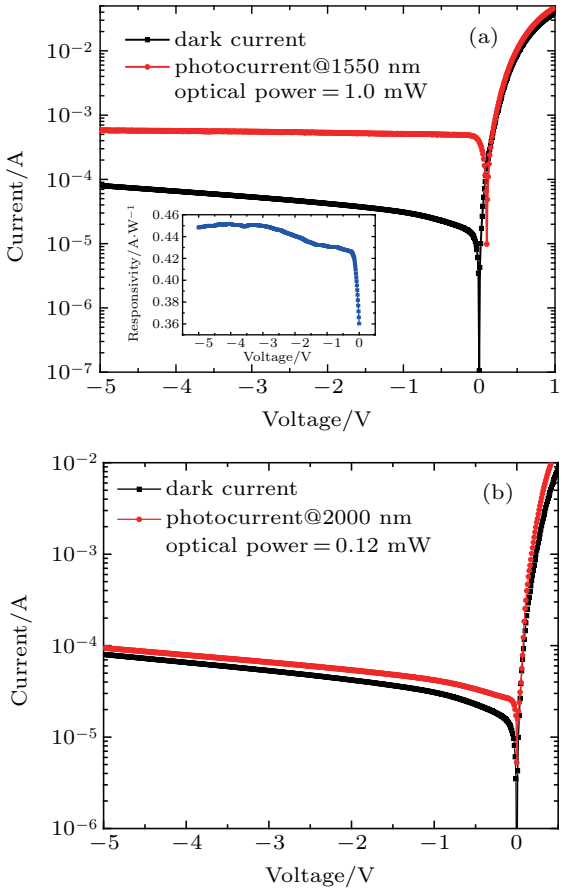


Fig. 5. Dark current and photocurrent illuminated by (a) 1550 nm (inset: responsivity of the detector as a function of bias voltage at 1550 nm), and (b) 2000 nm laser (optical power is 0.12 mW). The measured detector is 200 μm in diameter.

3.3. Photocurrent spectrum

The optical spectral response (1100–2500 nm) of the GeSn photodetector is shown in Fig. 6. The scatter plot, which was measured by a 1500–1630 nm tunable laser and a 2 μm laser under 3 V reverse bias voltage, has a good agreement with the optical spectral response measured by the FTIR optical spectrometer at 3 V reverse bias voltage. The response of the GeSn photodetector rapidly decreases as the wavelength increases until the wavelength reaches about 1640 nm, which exactly corresponds to the direct-bandgap of tensile-strain Ge.[1,2] As the wavelength increases further, the response of the GeSn photodetector begins to increase, which attributes to the absorption of the $Ge_{0.94}Sn_{0.06}$ absorbing layer

and the Ge indirect-bandgap. Furthermore, there is a sharp decline of response at 1810 nm and the spectral response finally arrives a cutoff at the wavelength about 2.3 μm. This greatly extended cutoff wavelength is the result of the narrow bandgap of GeSn caused by the incorporation of Sn and almost fully strain-relaxed GeSn layer.

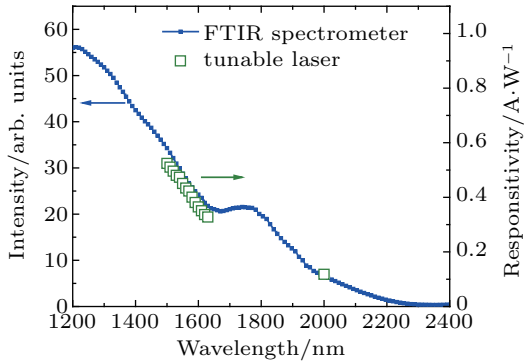


Fig. 6. Optical responsivity and spectrum response of GeSn photodetector as a function of wavelength. Devices were measured by lasers (a tunable laser between 1500 nm to 1630 nm, a laser at 2000 nm) and an FTIR optical spectrometer. The data are shown in green scatter plots and blue curve, respectively (all measurements were conducted under 3 V reverse bias voltage).

4. Conclusion

In summary, the high-quality GeSn layer was grown by MBE combined with multiple cycle annealing technology and fabricated into the silicon-based $Ge_{0.94}Sn_{0.06}$ p–i–n photodetectors adopting a CMOS compatible manufacturing process. This GeSn photodetector achieved a responsivity as high as 0.45 A/W at 1550 nm and 0.12 A/W at 2 μm. The wide spectrum detection with cutoff wavelength of 2.3 μm and dark-current density as low as 0.078 A/cm^2 under a bias of −1 V were achieved. This work shows a prospective method to fabricate GeSn p–i–n photodetectors and has great importance in silicon-based short-wave infrared detection and developing cost-effective monolithically integrated Si photonics.

References

[1] Eckhardt C, Hummer K and Kresse G 2014 *Phys. Rev. B* **89** 165201
[2] Du W, Ghetmiri S A, Conley B R, Mosleh A, Nazzal A, Soref R A, Sun G, Tolle J, Margetis J, Naseem H A and Yu S Q 2014 *Appl. Phys. Lett.* **105** 051104
[3] Han G Q, Wang Y B, Liu Y, Zhang C F, Feng Q, Liu M S, Zhao S L, Cheng B W, Zhang J C and Hao Y 2016 *IEEE Electron. Dev. Lett.* **37** 701
[4] Hansen M P and Malchow D S 2008 *Proceedings of SPIE-The International Society for Optical Engineering*, March 18–20, 2008, Orlando, FL, USA, U82–U92
[5] Soref R, Buca D and Yu S Q 2016 *Opt. Photon. News.* **27** 32
[6] Bauer M R, Cook C S, Aella P, Tolle J, Kouvetakis J, Crozier P A, Chizmeshya A V G, Smith D J and Zollner S 2003 *Appl. Phys. Lett.* **83** 3489
[7] Gassenq A, Gencarelli F, Campenhout J V, Shimura Y, Loo R, Narcy G, Vincent B and Roelkens G 2012 *Opt. Express* **20** 27297
[8] Kasper E, Kittler M, Oehme M and Arguirov T 2013 *Photon. Res.* **1** 69
[9] Kouvetakis J, Menendez J and Chizmeshya A V G 2006 *Annu. Rev. Mater. Res.* **36** 497
[10] Wang W, Su S J, Zheng J, Zhang G Z, Zuo Y H, Cheng B W and Wang Q M 2011 *Chin. Phys. B* **20** 068103
[11] Zhang Z P, Song Y X, Zhu Z Y S, Han Y, Chen Q M, Li Y Y, Zhang L Y and Wang S M 2017 *Aip. Adv.* **7** 045211
[12] Bauer M R, Tolle J, Bungay C, Chizmeshya A V G, Smith D J, Menéndez J and Kouvetakis J 2003 *Solid. State. Commun.* **127** 355
[13] Zaima S, Nakatsuka O, Taoka N, Kurosawa M, Takeuchi W and Sakashita M 2015 *Sci. Technol. Adv. Mat.* **16** 043502
[14] Luan H C, Lim D R, Lee K K, Chen K M, Sandl, J G, Wada K and Kimerling L C 1999 *Appl. Phys. Lett.* **75** 2909
[15] Mathews J, Roucka R, Xie J, Yu S Q, Menéndez J and Kouvetakis J 2009 *Appl. Phys. Lett.* **95** 133506
[16] Tseng H H, Li H, Mashanov V, Yang Y J, Cheng H H, Chang G E, Soref R A and Sun G 2013 *Appl. Phys. Lett.* **103** 231907
[17] Zheng J, Wang S, Liu Z, Cong H, Xue C L, Li C B, Zuo Y H, Cheng B W and Wang Q M 2016 *Appl. Phys. Lett.* **108** 033503
[18] Dong Y, Wang W, Lei D, Gong X, Zhou Q, Lee S Y, Loke W K, Yoon S F, Tok E S, Liang G and Yeo Y C 2015 *Opt. Express* **23** 18611
[19] Zhang D L, Xue C L, Cheng B W, Su S J, Liu Z, Zhang X, Zhang G Z, Li C B and Wang Q M 2013 *Appl. Phys. Lett.* **102** 141111
[20] Conley B R, Mosleh A, Ghetmiri S A, Du W, Soref R A, Sun G, Margetis J, Tolle J, Naseem H A and Yu S Q 2014 *Opt. Express* **22** 15639
[21] Cong H, Xue C L, Zheng J, Yang F, Yu K, Liu Z, Zhang X, Cheng B W and Wang Q M 2016 *IEEE Photon. J.* **8** 1
[22] Gassenq A, Gencarelli F, Campenhout J V, Shimura Y, Loo R, Narcy G, Vincent B and Roelkens G 2012 *Opt. Express* **20** 27297
[23] Xu S Q, Huang Y C, Wang W, Dong Y, Masudy-Panah S, Guo X, Wang H, Gong X and Yeo Y C 2018 *IEEE International Conference on Group IV Photonics*, August 29–31, 2018, Cancun, Mexico, p. 139
[24] Pham T, Du W, Tran H, Margetis J, Tolle J, Sun G, Soref R A, Naseem H A, Li B and Yu S Q 2016 *Opt. Express* **24** 4519
[25] Tran H, Pham T, Du W, Zhang Y, Grant P C, Grant J M, Sun G, Soref R A, Margetis J, Tolle J, Li B, Mortazavi M and Yu S Q 2018 *J. Appl. Phys.* **124** 013101
[26] Ye K, Zhang W, Oehme M, Schmid M, Gollhofer M, Kostecki K, Widmann D, Körner R, Kasper E and Schulze J 2015 *Solid. State. Electron.* **110** 71
[27] Conley B R, Mosleh A, Ghetmiri S A, Du W, Soref R A, Sun G, Margetis J, Tolle J, Naseem H A and Yu S Q 2014 *Opt. Express* **22** 15639
[28] Pham T, Conley B R, Margetis J, Tran H, Ghetmiri S A, Mosleh A, Du W, Sun G, Soref R A, Tolle J, Naseem H A, Li B H and Yu S Q 2015 *Conference on Lasers and Electro-optics*, May 10–15, 2015, San Jose, CA, USA, STh1I.7
[29] Liu J, Cannon D D, Wada K, Ishikawa Y, Danielson D T, Jongthammanurak S, Michel J and Kimerling L C 2004 *Phys. Rev. B* **70** 155309
[30] Oehme M, Schmid M, Kaschel M, Gollhofer M, Widmann D, Kasper E and Schulze J 2012 *Appl. Phys. Lett.* **101** 141110
[31] Su S J ,Cheng B W, Xue C L, Wang W, Cao Q, Xue H Y, Hu W X, Zhang G Z, Zuo Y H and Wang Q M 2011 *Opt. Express* **19** 6408
[32] Lu C M, Lee C H, Nishimura T and Toriumi A 2015 *Appl. Phys. Lett.* **107** 072904
[33] Morea M, Brendel C E, Zang K, Suh J, Fenrich C S, Huang Y C, Chung H, Huo Y, Kamins T I, Saraswat K C and Harris J S 2017 *Appl. Phys. Lett.* **110** 091109
[34] Huang B J, Lin J H, Cheng H H and Chang G E 2018 *Opt. Lett.* **43** 1215
[35] Zheng J, Liu Z, Xue C L, Li C B, Zuo Y H, Cheng B W and Wang Q M 2018 *J. Semicond.* **39** 061006
[36] Oehme M, Kostecki K, Schmid M, Kaschel M, Gollhofer M, Ye K, Widmann D, Koerner R, Bechler S, Kasper E and Schulze J 2014 *Appl. Phys. Lett.* **104** 161115